

Visualization and interpretation of attosecond electron dynamics in laser-driven hydrogen molecular ion using Bohmian trajectories

Norio Takemoto^{a)} and Andreas Becker

JILA and Department of Physics, University of Colorado, 440 UCB, Boulder, Colorado 80309-0440, USA

(Received 4 December 2010; accepted 18 January 2011; published online 16 February 2011)

We analyze the attosecond electron dynamics in hydrogen molecular ion driven by an external intense laser field using the Bohmian trajectories. To this end, we employ a one-dimensional model of the molecular ion in which the motion of the protons is frozen. The Bohmian trajectories clearly visualize the electron transfer between the two protons in the field and, in particular, confirm the recently predicted attosecond transient localization of the electron at one of the protons and the related multiple bunches of the ionization current within a half cycle of the laser field. Further analysis based on the quantum trajectories shows that the electron dynamics in the molecular ion can be understood via the phase difference accumulated between the Coulomb wells at the two protons. © 2011 American Institute of Physics. [doi:10.1063/1.3553178]

I. INTRODUCTION

The causal interpretation of quantum mechanics by de Broglie and Bohm provides the concept of trajectories for the dynamics of microscopic objects.^{1,2} These trajectories, called Bohmian trajectories or quantum trajectories, are navigated by the wavefunction. Conversely, if we regard the probability density (i.e., the squared modulus of the wavefunction) of the system as a fluid, the flow of this fluid can be elucidated by the quantum trajectories.^{3,4} It is this characteristics of the Bohmian trajectories that we want to utilize in this article to visualize and analyze a recently revealed counter-intuitive electronic motion in H_2^+ molecular ion exposed to intense laser light on an attosecond time scale.⁵⁻⁷

Previously, we found in *ab initio* numerical simulations that H_2^+ at intermediate internuclear distances (i.e., between the equilibrium distance and the dissociation limit) in an intense infrared laser pulse shows multiple bursts of ionization within a half-cycle of the laser field oscillation.⁷ This ionization dynamics contradicts the widely accepted picture of strong-field ionization, namely that an electron leaves the atom or molecule with largest probability at the peaks of the oscillating electric field of the laser. For example, in the often used tunnel ionization picture the electron tunnels through the barrier created by the binding potential of the ionic core and the electric potential of the laser field. This tunnel barrier is, of course, thinnest when the electric field strength is strongest, which leads to the above mentioned expectation for the most likely time instants of the electron escape. We identified that the unexpected multiple ionization bursts are induced by a previously reported ultrafast transient localization of the electron density at one of the protons.⁵ This attosecond dynamics can cause that the electron density near the tunnel barrier in the molecular ion is highest when the external field strength is below its peak strength. Correspondingly, the electron does not tunnel most likely at the maxima of the field but at other time instants.

^{a)}Electronic mail: norio@jilau1.colorado.edu.

We confirmed and extended earlier interpretations^{5,8} that the internal dynamics of the electron is a result of a strong and exclusive trapping of the population within a pair of states of opposite parity, so-called charge resonant states.⁹ Consequently, the attosecond localization dynamics of the electron in the hydrogen molecular ion driven by the laser field can be successfully reproduced using a two-state model.⁷ The dynamics can be understood also by the phase-space flow of the electron probability density regulated through the so-called momentum gates which are shifted in time by the vector potential of the external laser field.⁶

However, results of numerical simulations for the flow of the electron probability density often do not reveal many details and cannot provide much further insights into the internal electron dynamics in the molecular ion. We therefore use the concept of Bohmian trajectories to provide a complementary picture of the dynamics. By analyzing the motion of the trajectories, we furthermore clarify that it is the phase difference of the local wavefunctions at the two protons that is the origin of the force, which is sometimes driving the electron in the direction opposite to the strong electric field of the laser light.

We note here that the Bohmian mechanics has attracted much attention in the last decade as a basis of developing new and efficient methods for simulating the time evolution of a quantum system.^{4,10-14} This resurgence of attention was initiated by the demonstrations that the time-evolving phase and amplitude of a wavefunction can be calculated over the course of the Bohmian trajectories for which a closed-set of equations of motion were derived.^{10,11} Thus, it was shown that the wavefunction can be synthesized from the Bohmian trajectories rather than solving the time-dependent Schrödinger equation (TDSE) itself on a set of grid points fixed in space. In the present work, however, we use the traditional method to calculate the Bohmian trajectories from the wavefunction obtained by solving TDSE.³ In this way, we assure that the resultant Bohmian trajectories correctly visualize the flow of the probability density, and we can focus on the analysis of

the properties (especially, the velocity) of the Bohmian trajectories.

The rest of the paper is organized as follows. In Sec. II, we present the model for H_2^+ used for our analysis. In Sec. III, we present the results for the Bohmian trajectories and compare them with those for the electron probability densities obtained from *ab initio* numerical simulations. We identify the phenomena of transient electron localization and multiple ionization bursts in the time evolution of the trajectories. In Sec. IV, we make use of the Bohmian trajectory calculations to provide an analysis of the sometimes counter-intuitive electron dynamics in the hydrogen molecular ion. Finally, Sec. V concludes the paper.

II. THEORY

In recent studies of laser induced dynamics of the hydrogen molecular ion, the full three-dimensional (3D) electronic motion (e.g., Ref. 15) or the two degrees-of-freedom electronic motion in cylindrical coordinates (e.g., Refs. 5,16–18) along with one-dimensional (1D) nuclear motion have been taken into account. In the present study, we consider a simpler 1D model for the electronic dynamics of H_2^+ in which the positions of the protons are fixed in space. We have shown that the electron localization dynamics inside the molecular ion as well as the phenomenon of multiple ionization bursts does not change in higher dimensional models.^{7,19} In particular, we found that the nonadiabatic coupling between the electronic and nuclear motions is not essential for the internal electron dynamics. Also, use of the soft-core potential in the 1D model does not alter the essence of the dynamics, although there may be a discrepancy from the actual 3D Coulombic system at a quantitative level.²⁰ In fact, the attosecond electron localization in (model) hydrogen molecular ion has been reported in all the cases of Coulombic potential in 3D,⁵ soft-core potential in 3D,⁶ and soft-core potential in 1D.⁷

A. 1D fixed-nuclei model of H_2^+

In our 1D model of H_2^+ with fixed positions of the protons, the internuclear axis was assumed to be parallel to the polarization direction of the linearly polarized laser light. The Hamiltonian of this model system is given by (Hartree atomic units, $e = m = \hbar = 1$, are used throughout this article unless noted otherwise)

$$H(t) = -\frac{1}{2} \frac{\partial^2}{\partial z^2} + V_C(z; R) + V_L(z, t), \quad (1)$$

where z is the electron position measured from the center-of-mass of the two protons, which are separated by the distance R . The Coulomb interaction between the electron and the two protons was approximated by the soft-core potential,^{21,22}

$$V_C = -\frac{1}{\sqrt{(z+R/2)^2+a}} - \frac{1}{\sqrt{(z-R/2)^2+a}}, \quad (2)$$

where a is the soft-core parameter. The laser-electron interaction was expressed in the length gauge as

$$V_L(z, t) = zE(t). \quad (3)$$

The laser electric field $E(t)$ is related to the vector potential $A(t)$ by

$$\begin{aligned} E(t) &= -\frac{\partial A(t)}{\partial t} \\ &= -\frac{\partial f_A(t)}{\partial t} \sin \left[\omega \left(t - \frac{T}{2} \right) + \varphi \right] \\ &\quad - f_A(t) \omega \cos \left[\omega \left(t - \frac{T}{2} \right) + \varphi \right], \end{aligned} \quad (4)$$

where we used the following form of the vector potential:

$$A(t) = f_A(t) \sin \left[\omega \left(t - \frac{T}{2} \right) + \varphi \right], \quad (5)$$

$$f_A(t) = \begin{cases} A_0 \sin^2(\pi t/T) & (0 \leq t \leq T) \\ 0 & (\text{otherwise}) \end{cases}. \quad (6)$$

The full-width at half-maximum (FWHM) of this envelope function, $f_A(t)$, is equal to $T/2$.

B. Propagation of the wavefunction and the quantum trajectories

With the Hamiltonian given as above, the wavefunction $\Psi(z, t)$ was propagated according to the corresponding TDSE,

$$i \frac{\partial}{\partial t} \Psi(z, t) = H(t) \Psi(z, t). \quad (7)$$

This TDSE was solved numerically using the second-order split-operator method on the Fourier grid.^{23–25} The spatial and temporal grid intervals used for the simulations were $\Delta z = 0.152$ and $\Delta t = 0.0245$ or smaller.

At the same time as the wavefunction $\Psi(z, t)$ was propagated in time, the Bohmian trajectories $\{z_j(t) | j = 1, \dots, N_{\text{traj}}\}$ were propagated as well by solving the equation of motion,

$$\frac{dz_j}{dt} = v(z_j(t), t), \quad (8)$$

where the velocity field $v(z, t)$ is given by the phase gradient of the wavefunction,

$$\Psi(z, t) = C(z, t) \exp(iS(z, t)) \quad (9)$$

with $C \geq 0$ and $S \in \mathbb{R}$, as

$$v(z, t) = \frac{\partial S}{\partial z}. \quad (10)$$

The following identity was utilized in the actual computation:

$$\frac{\partial S}{\partial z} = \text{Im} \left[\frac{1}{\Psi} \frac{\partial \Psi}{\partial z} \right]. \quad (11)$$

The ordinary differential equation (8) with respect to t was solved by the fourth order Runge–Kutta scheme²⁶ with the fixed step size of $2\Delta t$, i.e., twice the time step of the wavefunction propagation. The wavefunction value at every other step of its propagation was used to evaluate the velocities of the trajectories at the mid-point of one Runge–Kutta step to achieve the fourth order accuracy. We may note parenthetically that expression (10) for the velocity field is valid for the wavefunction in the length gauge representation used in the

present study. In the velocity gauge representation, the velocity field is given by $v(z, t) = \partial S / \partial z - A(t)$.³

The initial positions of the quantum trajectories were distributed at a regular interval, δz , and for each trajectory we assigned the weight,

$$w_j = \int_{\Omega_j(t_0)} dz |\Psi(z, t_0)|^2, \quad (12)$$

$$\Omega_j(t_0) = \left\{ z \left| z_j(t_0) - \frac{\delta z}{2} < z < z_j(t_0) + \frac{\delta z}{2} \right. \right\}. \quad (13)$$

At the limit of $\delta z \rightarrow 0$, we may consider that the weight w_j assigned at the initial time ($t = t_0 = 0$) is conserved over the time evolution.^{27,28}

III. VISUALIZATION OF THE INTERNAL ELECTRON DYNAMICS

In this section, we first compare the result of the Bohmian trajectory calculation with electron probability density obtained by integrating the TDSE for the 1D H_2^+ model initially prepared in its ground state and brought to interaction with a linearly polarized intense laser pulse. For this exemplary comparison, we have chosen the distance between the two protons as $R = 7$ and considered a laser pulse with a peak intensity of 4×10^{13} W/cm², a wavelength of 1064 nm, a full duration of $T = 10$ cycles, and a carrier-to-envelope phase (CEP) of $\varphi = 0$. We set the soft-core parameter as $a = 2.0$ so that the energies of the ground and first-excited electronic states of the 1D model (-0.519 and -0.491 , including the $1/R$ nuclear repulsion) best reproduce the exact values (-0.506 and -0.496) (Ref. 29) for the actual H_2^+ in 3D space at $R = 7$. The initial positions of 100 quantum trajectories were distributed over $-10 \leq x \leq 10$ at a regular interval $\delta z = 0.202$, and their weights $\{w_j\}$ were determined via Eq. (12).

In Fig. 1, the Bohmian trajectories [Fig. 1(a)] are presented along with the electron probability density

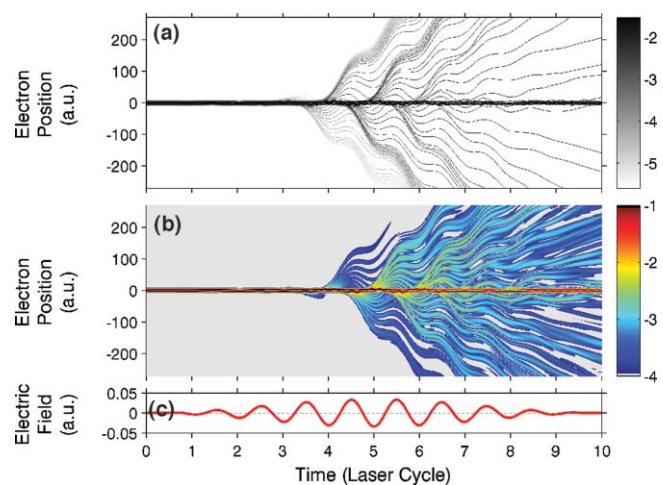


FIG. 1. Comparison of the quantum trajectories (a) and the electron probability density (b) for the 1D model of H_2^+ at $R = 7$ for the interaction of H_2^+ with the electric field (c) of a laser pulse (peak intensity 4×10^{13} W/cm², wavelength 1064 nm, duration $T = 10$ cycles, and CEP $\varphi = 0$). In panel (a), the gray-scale color of each trajectory indicates $\log_{10} w_j$. In panel (b), the color code indicates $\log_{10} |\Psi|^2$, where Ψ is obtained by solving the TDSE (7).

[Fig. 1(b)] as a function of time. For the sake of comparison, the electric field of the laser pulse is shown in Fig. 1(c) as well. Subject to the intense electric field, the trajectories leave the core region (at $z \approx 0$) of the molecular ion in alternating directions ($z \rightarrow \pm\infty$) at every half cycle of the laser field. It is clearly seen that the number of ionizing trajectories increases as the field strength increases during the laser pulse. The trajectories liberated from the core region show wiggling motion forced by the alternating electric field of the laser. Due to this quiver motion, some of the trajectories, depending on the time instants of their release, are driven back to the core region and scattered off the protons. Please note that the result for the Bohmian trajectories visually agree very well with that for the electron probability density: regions of large probability density correspond to a large density of the Bohmian trajectories. Thus, the Bohmian trajectories provide a complete overall picture of the ionization process, including the quiver motion and the rescattering of the electron in the laser field. This agrees with the findings of earlier studies using Bohmian trajectories to describe the interaction of atoms with intense laser pulses.^{14,30–32}

In Figs. 2(a)–2(c), we show a detailed view of the quantum trajectory motion in and close to the core region (the protons are located at $z = \pm R/2 = \pm 3.5$) over the central field cycle ($T/2 - 2\pi/\omega < t < T/2 + 2\pi/\omega$) of the laser pulse. The laser electric field in the same time window is also shown in Fig. 2(d). In the simulation for Fig. 2(a), the wavefunc-

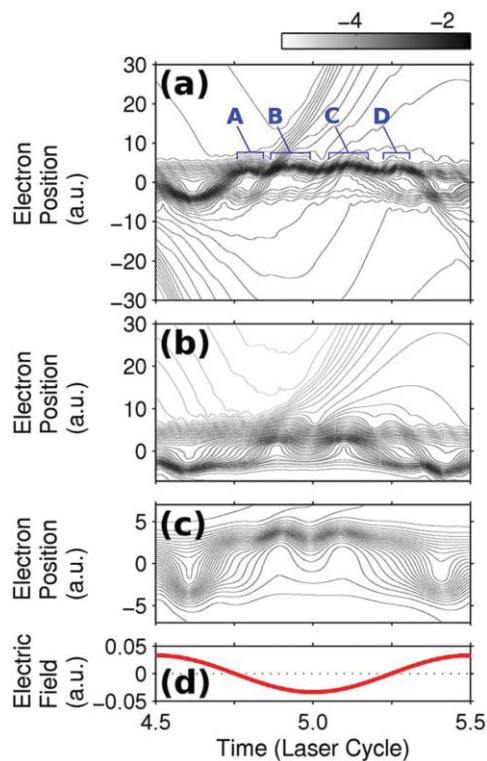


FIG. 2. Close-up view on the time evolution of the quantum trajectories (a–c) over the single laser cycle at the pulse peak. The laser electric field is shown in panel (d) for comparison with the motion of the quantum trajectories. In panel (a), no wavepacket absorber was set close to the core region. In panel (b), an absorber was set on one side of the core region at $-11 < z < -7$. In panel (c), two absorbers were set on both sides of the core region at $7 < |z| < 11$.

tion masks of $\cos^{1/4}$ -shape were placed over $270 < |z| < 300$ only to avoid the reflection of the ionized wavepackets at the boundaries of the large simulation box, leaving the electron dynamics in the region of z shown in this panel unaffected. The quantum trajectories show an ultrafast oscillatory motion around the core, $|z| < 10$, and they are pushed outward from $z = R/2$ for the durations marked by A-D in Fig. 2(a). These outward motion may involve the direct ionization and rescattering of the electron. To separate these two types of processes, we suppressed the rescattering effect on the negative z -side by setting a wavefunction mask at $-11 < z < -7$ for the simulations in Fig. 2(b).^{7,33-35} As a result, the peak A in Fig. 2(a) disappears in Fig. 2(b), indicating that this peak was created by the wavepacket driven back from $z < 0$ and passing through the core region toward $z > 0$. In Fig. 2(c), the wavefunction masks were set close to the core on both sides (at $7 < |z| < 11$), and all the rescattering wavepackets were absorbed after the initial ionization. The two peaks B and C in Fig. 2(a) are still present in Fig. 2(c) while peak D disappears, indicating that there are actually two bursts of ionization under the present conditions. These results confirm the previously reported phenomena of multiple ionization bursts and attosecond electron localization.^{5,7}

The quantum trajectories in Fig. 2(c) clearly elucidate that the electron probability transfers back and forth between the two protons on the ultrafast time scale shorter than a half-cycle of the laser field. This motion has not been as obvious in the plot of the electron probability density in the previous studies.^{5,7} Please note that the electronic motion in Fig. 2(c) between the two potential wells created by the protons does not necessarily follow the laser-electron interaction potential V_L . For example, at $t = 5$ cycles, the oscillating laser electric field $E(t)$ is peaked in the negative direction [cf., Fig. 2(d)], and hence the slope of V_L pushing the electron toward $z \rightarrow +\infty$ becomes maximum. Nevertheless, for a short time before $t = 5$ cycles, we observe some bound trajectories propagate in the opposite direction from the proton located at $z = R/2 = 3.5$ to the other one at $z = -R/2 = -3.5$ by climbing up the potential V_L . This counter-intuitive (and classically forbidden) motion of the electron was noticed first in the context of coherent control of electron localization in dissociating H_2^+ molecule by the Wigner representation.⁶ The present results confirm this motion and visualize it using Bohmian trajectories.

IV. ANALYSIS OF THE ELECTRON DYNAMICS USING BOHMIAN TRAJECTORIES

We have seen so far that the Bohmian trajectories clearly visualize the transient electron localization and multiple ionization bursts within a half-cycle of the laser field oscillation. In this section, we will now investigate the origin of the counter-intuitive motion of the Bohmian trajectories. To this end, we focus on the results for the intra-molecular electron transfer from one proton to the other, obtained by using the wavepacket absorbers over $7 < |z| < 11$ in order to eliminate the effect of rescattering wavepackets [cf., Fig. 2(c)].

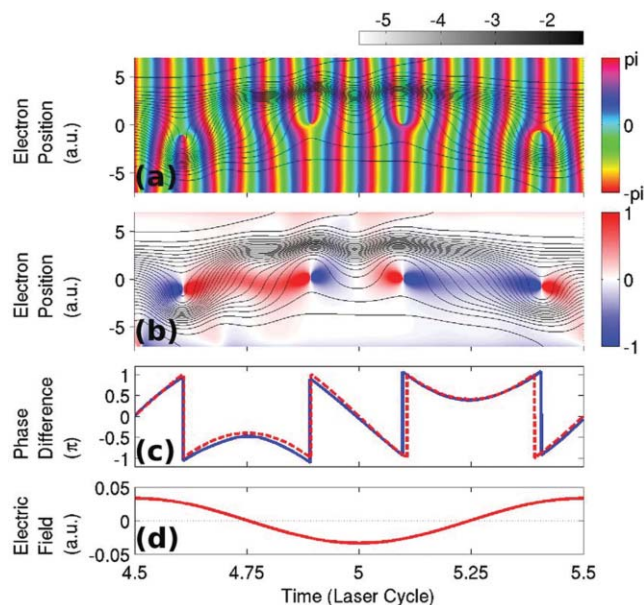


FIG. 3. Analysis of the intra-molecular motion of the quantum trajectories in terms of the phase of the wavefunction and the velocity field. (a) Phase $S(z, t)$ and the quantum trajectories $\{z_j(t)\}$. (b) Velocity field $v(z, t)$ and the quantum trajectories $\{z_j(t)\}$. (c) Phase difference between the two wells calculated from the 1D model $[\alpha_{\text{lr}}(t)]$, blue solid line] and from the approximate solution of the two-state model $[\alpha_{\text{lr}}^{(2\text{lev})}(t)]$, red dashed line]. (d) Electric field of the laser pulse (wavelength 1064 nm, peak intensity 4×10^{13} W/cm², duration $T = 10$ cycles, and CEP $\varphi = 0$).

A. Velocity field for the Bohmian trajectories

As pointed out before, we observe that some of the trajectories turn their direction toward $z < 0$ near the peak of the electric field at $t = 5$ cycles, while the classical force due to the laser electric field pushes the electron in the positive z direction. We now investigate this counter-intuitive motion in terms of the velocity field, $v(z, t) = \partial S(z, t) / \partial z$, for the Bohmian trajectories. Figure 3(a) shows the phase $S(z, t)$ of the wavefunction as a function of time and electron position. The 2π -periodicity of the wavefunction phase is faithfully represented by the cyclic hue of the colors. Figure 3(b) shows the velocity field $v(z, t)$. These were calculated using the same parameters of the laser field as before. In both figures, we superposed the Bohmian trajectories for further visualization.

From Fig. 3(a), we can notice that at a given time instant the phase of the wavefunction is almost constant for z within each of the potential wells. However, the phase propagates at different speeds in the two wells. This causes a phase gradient around $z = 0$ and, consequently, a large absolute value of the velocity field in the region between the protons. Based on this observation, we may expect the sign of $v = \partial S / \partial z$ around $z = 0$ to be the same as $S(z = R/2) - S(z = -R/2)$. The solid blue curve in Fig. 3(c) shows the phase difference defined as

$$\alpha_{\text{lr}}(t) = \arg \left[\Psi \left(z = -\frac{R}{2}, t \right) \right] - \arg \left[\Psi \left(z = \frac{R}{2}, t \right) \right], \quad (14)$$

and the sign of $-\alpha_{\text{lr}}(t)$ indeed agrees with that of v .

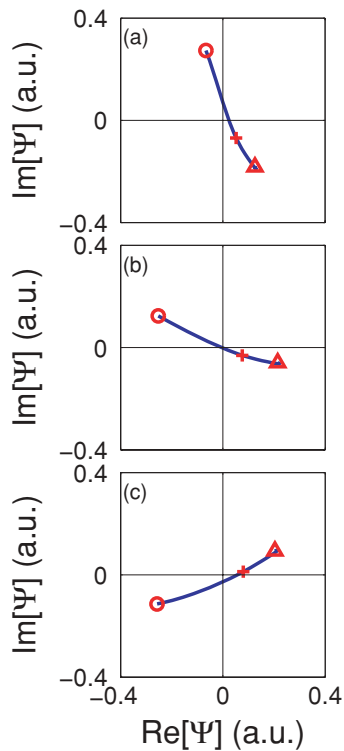


FIG. 4. Wavefunction $\Psi(z, t)$ is plotted in the complex Ψ -plane at (a) $t = 4.60$ laser cycles, (b) $t = 4.61$ laser cycles, and (c) $t = 4.62$ laser cycles by taking the position coordinate $z \in [-R/2, R/2]$ as the parameter. The red circle, cross, and triangle in each panel indicate the wavefunction values at $z = -R/2, 0$, and $R/2$, respectively.

In Fig. 3(c), the relative phase $\alpha_{lr}(t)$ changes its sign either by continuously passing through $\alpha_{lr} = 0$ (at $t = 4.5, 5.0$, and 5.5 laser cycles) or by jumping between $\alpha_{lr} \approx \pm\pi$ (at $t = 4.61, 4.89, 5.10$, and 5.41 laser cycles). At the time instants corresponding to both types of sign change, the Bohmian trajectories are forced to turn their direction. However, comparison of Fig. 3(c) with the Bohmian trajectories in Figs. 3(a) and 3(b) reveals that the sign change due to the abrupt phase jump causes the attosecond transient electron localization.

In Fig. 4, we illustrate the cause of the phase jump by plotting the wavefunction on the complex Ψ -plane by taking the position coordinate $-R/2 \leq z \leq R/2$ as the parameter at three instants around the phase jump at $t = 4.61$ laser cycles. Before the jump [Fig. 4(a)], we see that the phase at $z = -R/2$ (circle) is larger than $z = R/2$ (triangle). At the instant of the jump [Fig. 4(b)], the Ψ -curve passes through the origin, i.e., a node $|\Psi| = 0$ is developed. At the position of the node, the phase is undefined, and hence the relative phase α_{lr} also becomes undefined temporarily. However, at the next moment [Fig. 4(c)], the Ψ -curve has crossed the origin since the phase at $z = -R/2$ accumulates faster than the phase at $z = R/2$. At this time, the phase at $z = -R/2$ is smaller than that at $z = R/2$. Intuitively speaking, if the local phase at one well becomes more and more advanced (or retarded) from that at the other well and the phase difference approaches π (or $-\pi$), then the Ψ -curve becomes almost straight (as in Fig. 4) and passes through the origin at some instant. At this moment, the advanced-retarded relation of the

local phases at the two wells interchanges. Before concluding this section, we should note that the jump of the relative phase α_{lr} causes a sudden change of $v(z, t)$ between $\pm\infty$. However, this divergence of $v(z, t)$ is accompanied by a node of the wavefunction, and therefore the flux $v(z, t)|\Psi(z, t)|^2$ stays finite.

B. Phase difference in two-state model

Next, we show that the phase difference $\alpha_{lr}(t)$ can be approximated by a simple expression based on a two-state model. To this end, we analyze the relative phase between the two potential wells in terms of the following localized states,^{36–38}

$$|l\rangle = \frac{1}{\sqrt{2}} [|g\rangle + |u\rangle], \quad (15)$$

$$|r\rangle = \frac{1}{\sqrt{2}} [|g\rangle - |u\rangle], \quad (16)$$

where $|g\rangle$ and $|u\rangle$ are the ground and first-excited electronic states, respectively, of the 1D fixed-nuclei model. Without loss of generality, we set the phases of $|g\rangle$ and $|u\rangle$ such that $|l\rangle$ and $|r\rangle$ are localized at $z = -R/2$ and $z = R/2$, respectively. By approximating the state of the system in the basis of these two localized states as $|\Psi(t)\rangle = c_l(t)|l\rangle + c_r(t)|r\rangle$, the time evolution of $c_l(t)$ and $c_r(t)$ is given by

$$i \frac{d}{dt} \begin{pmatrix} c_l \\ c_r \end{pmatrix} = \left[H_0^{(2\text{lev})} + V_L^{(2\text{lev})} \right] \begin{pmatrix} c_l \\ c_r \end{pmatrix}, \quad (17)$$

with the field-free Hamiltonian

$$H_0^{(2\text{lev})} = -\frac{\Delta_0}{2} \begin{pmatrix} 0 & 1 \\ 1 & 0 \end{pmatrix}, \quad (18)$$

and the interaction potential

$$V_L^{(2\text{lev})} = -d_{gu}E(t) \begin{pmatrix} 1 & 0 \\ 0 & -1 \end{pmatrix}, \quad (19)$$

where Δ_0 is the absolute value of the difference between the field-free energies of $|u\rangle$ and $|g\rangle$, and $d_{gu} = -\langle g|z|u\rangle \geq 0$ is the transition dipole moment between $|g\rangle$ and $|u\rangle$.

If the laser-molecule coupling $|d_{gu}E(t)|$ is sufficiently strong and/or the laser frequency ω is sufficiently larger than the tunnel splitting Δ_0 , we may approximate the solution to the two-state TDSE (17) by taking $V_L^{(2\text{lev})}$ as the zeroth order reference Hamiltonian and omitting the $H_0^{(2\text{lev})}$ term.^{38–44} Such a zeroth order solution can be easily obtained as³⁸

$$c_l^{(0)}(t) = \exp \{ -i d_{gu} [A(t) - A(t_0)] \} c_l^{(0)}(t_0), \quad (20)$$

$$c_r^{(0)}(t) = \exp \{ i d_{gu} [A(t) - A(t_0)] \} c_r^{(0)}(t_0), \quad (21)$$

where the relation of the electric field and vector potential, Eq. (4), was used. Then, the phase difference between the two wells can be approximated by

$$\alpha_{lr}^{(2\text{lev})}(t) = \arg [c_l^{(0)}(t)] - \arg [c_r^{(0)}(t)]. \quad (22)$$

By substituting Eqs. (20) and (21) into Eq. (22), and noting that $A(t_0) = 0$ at the beginning of the laser pulse at $t = t_0 = 0$, we obtain

$$\alpha_{\text{lr}}^{(2\text{lev})}(t) = -2d_{\text{gu}}A(t) + \alpha_{\text{lr}}^{(2\text{lev})}(t_0). \quad (23)$$

The phase difference calculated by this expression is plotted in Fig. 3(c) with the red dashed line. It is presented in the $[-\pi, \pi]$ interval as we have already understood above that the relative phase stays approximately within this interval. We can see that the result of the two-state model closely reproduces the exact value (blue solid line) calculated numerically by Eq. (14).

The condition, $\alpha_{\text{lr}}^{(2\text{lev})}(t_{\text{turn}}) = n\pi$, $n \in \mathbb{Z}$, for the time instant t_{turn} at which the velocity field between the two protons changes its sign is then given by

$$A(t_{\text{turn}}) = \frac{-n\pi + \alpha_{\text{lr}}^{(2\text{lev})}(t_0)}{2d_{\text{gu}}}. \quad (24)$$

This expression has a similar form as the condition for the time instant t_{loc} of maximum electron localization,

$$A(t_{\text{loc}}) = \frac{m\pi + \chi}{2d_{\text{gu}}}, \quad (25)$$

where $m \in \mathbb{Z}$, derived previously⁷ based on the series expansion of the Floquet states for the two-state model.⁴⁴ In fact, these two expressions are identical at the limit of long laser pulse duration, where the mixing angle χ of the two Floquet states reduces to the initial phase difference $\alpha_{\text{lr}}^{(2\text{lev})}(t_0)$.

C. Origin of the counter-intuitive electron motion

The result of the two-state analysis in Subsection IV B, in which we consider $V_{\text{L}}^{(2\text{lev})}$ as the zeroth order Hamiltonian while neglecting the tunnel hopping term $H_0^{(2\text{lev})}$, provides us with an intuitive picture. Please note that the transition dipole moment has the asymptotic form $d_{\text{gu}} \sim R/2$ at large R ,⁹ and the difference of the diagonal elements of $V_{\text{L}}^{(2\text{lev})}$ is, hence, approximately equal to $RE(t)$, which is the difference of the electric potential induced by the laser field between the two wells. Using this asymptotic form of d_{gu} , the phase difference in Eq. (23) can be rewritten as

$$\alpha_{\text{lr}}^{(2\text{lev})}(t) \sim \int_{t_0}^t dt' RE(t') + \alpha_{\text{lr}}^{(2\text{lev})}(t_0). \quad (26)$$

This expression elucidates that the origin of the phase difference between the two potential wells, and hence the velocity field, is the difference of the electric potential energies between the two wells induced by the laser light.

This interpretation of the electronic dynamics based on the zeroth order two-state analysis predicts that the motion of the electron should be still counter-intuitive even at a relatively low intensity at which only one localization per half-cycle is predicted by Eq. (24) or (25). This is demonstrated in Fig. 5, in which the 1D model was initially prepared in the ground state, and a laser pulse of peak intensity 4×10^{12} W/cm² was applied. The other parameters were the same as above. The initial phase difference $\alpha_{\text{lr}}(t_0)$ is zero due to the choice of the initial state as $|g\rangle$, and the direction of the velocity field around $z = 0$ [Fig. 5(b)] evolves in time according

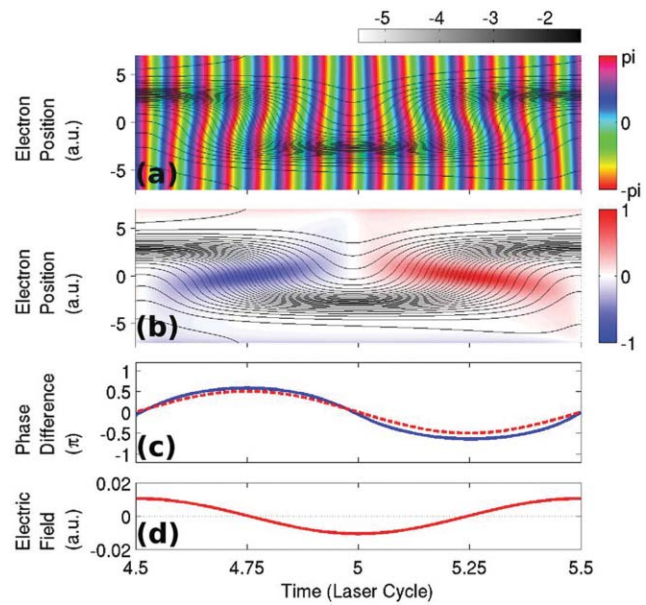


FIG. 5. Time evolutions of (a) the phase of the wavefunction and (b) the velocity field are plotted along with the quantum trajectories. The system was initially prepared in the ground state $|g\rangle$. Panel (c) shows the phase difference between the two local potential wells calculated from the TDSE solution (blue solid line) and from the two-state model (red dashed line). Panel (d) shows the electric field of the laser pulse (wavelength 1064 nm, peak intensity 4×10^{12} W/cm², duration $T = 10$ cycles, and CEP $\varphi = 0$).

to $-A(t)$ as predicted by the two-state analysis [Fig. 5(c)]. Due to the phase-lag between $A(t)$ and $E(t)$, the quantum trajectories are navigated from $z = R/2$ to $z = -R/2$ during the $4.5 < t < 5$, for example, while the electric force $-E(t)$ points in the opposite direction during $4.75 < t < 5$. As a consequence, the trajectories are always accumulated at the upper potential well, in contradiction to our classical intuition.

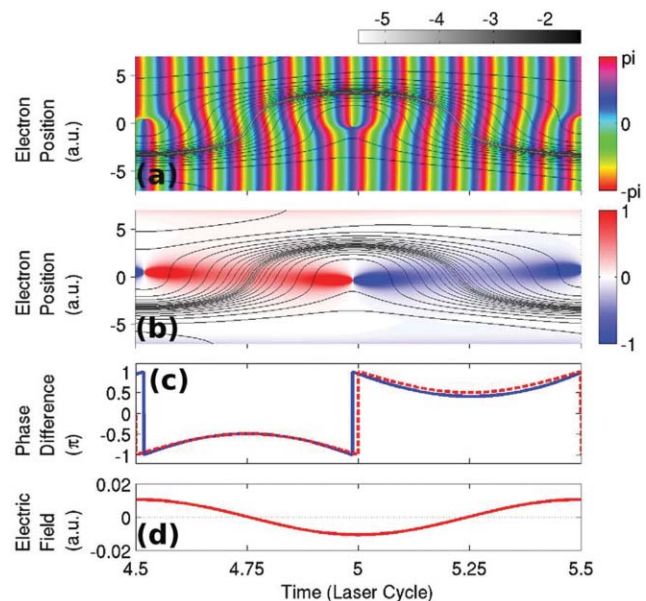


FIG. 6. Same as Fig. 5 except that here the system was initially prepared in the first excited state $|u\rangle$.

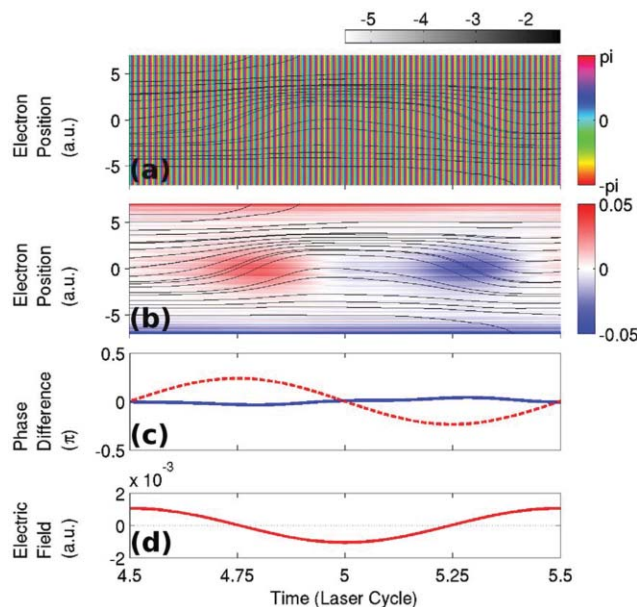


FIG. 7. Same as Fig. 5 except that here a laser pulse with long wavelength (5000 nm) and low intensity (4×10^{10} W/cm²) (duration $T = 10$ cycles, CEP $\varphi = 0$) was applied.

If, instead, the system is initially prepared in the first excited state $|u\rangle$, the initial phase difference $\alpha_{lr}(t_0) = -\pi$. Due to this offset, the quantum trajectories (and the electron probability density) should be navigated toward the lower potential well in this case. In fact, we can see that this is the case for the results presented in Fig. 6, where we applied the same laser pulse as used for the results shown in Fig. 5 but prepared the system in the 1D model of H_2^+ in the first excited state.

We may finally ask if there is a parameter regime in which our intuitive (classical) picture that the electron should move in the direction of the electric force is always recovered. As we mentioned above, our two-state analysis is based on the assumption that $V_L^{(2lev)}$ is the dominant term, i.e., that the laser-molecule coupling is strong and/or the photon energy is sufficiently larger than the tunnel splitting. Please note that the photon energy at the wavelength of 1064 nm is $\omega = 0.043$, whereas the tunnel splitting is $\Delta_0 = 0.028$ for the 1D model at $R = 7$. If we decrease the photon energy as well as the laser intensity, the two-state analysis is no longer applicable. In fact, the results in Fig. 7 show that at a wavelength of 5000 nm and an intensity of 4×10^{10} W/cm² our two-state analysis breaks down since the phase difference $\alpha_{lr}^{(2lev)}(t)$ (red dashed line) predicted by the two-state analysis deviates qualitatively from the value of $\alpha_{lr}(t)$ (blue solid line) calculated from the TDSE solution [Fig. 7(c)]. We can see that in this parameter regime, in which the conventional weak field perturbation theory may be applied, the motion of the quantum trajectories (and the electron probability density) follows the electric force of the laser field, and the intuitive (classical) picture is indeed recovered.

V. CONCLUSIONS

We have presented an analysis of the attosecond electron dynamics in hydrogen molecular ion driven by an

intense laser pulse in terms of Bohmian trajectory calculations using a 1D model. Recently predicted phenomena such as attosecond transient electron localization and multiple bursts of ionization within a half cycle of the laser pulse are clearly represented by the Bohmian trajectories. Further analysis let us identify the origin of the sometimes counter-intuitive motion of the Bohmian trajectories as due to the time-evolving phase difference of the wavefunction between the two potential wells induced by the electric potential of the laser field. We were able to predict the time instants at which the trajectories change their directions in terms of the simple two-state model. Following our analysis, we showed that, exposed to an intense laser field, the electron dynamics in the hydrogen molecular ion often does not follow the (classical) force of the laser electric field. Our classical expectations are, however, recovered in the perturbative weak-field limit in which the photon energy and intensity of the laser field are both sufficiently small.

ACKNOWLEDGMENTS

We acknowledge Professor H. Kono, Professor T. Kato, Dr. A. Picón, and A. Benseny for helpful discussions. This work was partially supported by the US National Science Foundation.

- ¹D. Bohm, *Phys. Rev.* **85**, 166 (1952).
- ²D. Bohm, *Phys. Rev.* **85**, 180 (1952).
- ³P. R. Holland, *The Quantum Theory of Motion: An Account of the de Broglie-Bohm Causal Interpretation of Quantum Mechanics* (Cambridge University Press, Cambridge, 1993).
- ⁴R. E. Wyatt, *Quantum Dynamics with Trajectories: Introduction to Quantum Hydrodynamics* (Springer, New York, 2005).
- ⁵I. Kawata, H. Kono, and Y. Fujimura, *J. Chem. Phys.* **110**, 11152 (1999).
- ⁶F. He, A. Becker, and U. Thumm, *Phys. Rev. Lett.* **101**, 213002 (2008).
- ⁷N. Takemoto and A. Becker, *Phys. Rev. Lett.* **105**, 203004 (2010).
- ⁸T. Zuo and A. D. Bandrauk, *Phys. Rev. A* **52**, R2511 (1995).
- ⁹R. S. Mulliken, *J. Chem. Phys.* **7**, 20 (1939).
- ¹⁰C. L. Lopreore and R. E. Wyatt, *Phys. Rev. Lett.* **82**, 5190 (1999).
- ¹¹F. S. Mayor, A. Askar, and H. A. Rabitz, *J. Chem. Phys.* **111**, 2423 (1999).
- ¹²B. Poirier, *Chem. Phys.* **370**, 4 (2010).
- ¹³Y. Goldfarb, I. Degani, and D. J. Tannor, *J. Chem. Phys.* **125**, 231103 (2006).
- ¹⁴P. Botheron and B. Pons, *Phys. Rev. A* **82**, 021404(R) (2010).
- ¹⁵S. X. Hu, L. A. Collins, and B. I. Schneider, *Phys. Rev. A* **80**, 023426 (2009).
- ¹⁶S. Chelkowski, T. Zuo, O. Atabek, and A. D. Bandrauk, *Phys. Rev. A* **52**, 2977 (1995).
- ¹⁷V. Roudnev, B. D. Esry, and I. Ben-Itzhak, *Phys. Rev. Lett.* **93**, 163601 (2004).
- ¹⁸F. He, C. Ruiz, and A. Becker, *Phys. Rev. Lett.* **99**, 083002 (2007).
- ¹⁹N. Takemoto and A. Becker, *Phys. Rev. A* (in preparation).
- ²⁰A. Kästner, F. Grossmann, and R. Schmidt, *Phys. Rev. A* **81**, 023414 (2010).
- ²¹J. Javanainen, J. H. Eberly, and Q. Su, *Phys. Rev. A* **38**, 3430 (1988).
- ²²K. C. Kulander, F. H. Mies, and K. J. Schafer, *Phys. Rev. A* **53**, 2562 (1996).
- ²³C. C. Marston and G. G. Balint-Kurti, *J. Chem. Phys.* **91**, 3571 (1989).
- ²⁴A. D. Bandrauk and H. Shen, *J. Chem. Phys.* **99**, 1185 (1993).
- ²⁵K. Takahashi and K. Ikeda, *J. Chem. Phys.* **99**, 8680 (1993).
- ²⁶W. H. Press, S. A. Teukolsky, W. T. Vetterling, and B. P. Flannery, *Numerical Recipes in Fortran 77: The Art of Scientific Computing, Vol. 1 of Fortran Numerical Recipes*, 2nd ed. (Cambridge University Press, New York, 1992).
- ²⁷S. Garashchuk and V. A. Rassolov, *Chem. Phys. Lett.* **364**, 562 (2002).
- ²⁸S. Garashchuk and V. A. Rassolov, *J. Chem. Phys.* **118**, 2482 (2003).

- ²⁹T. E. Sharp, *At. Data Nuc. Data Tables* **2**, 119 (1970).
- ³⁰F. H. M. Faisal and U. Schwengelbeck, *Pramana, J. Phys.* **51**, 585 (1998).
- ³¹X. Y. Lai, Q. Y. Cai, and M. S. Zhan, *Eur. Phys. J. D* **53**, 393 (2009).
- ³²X. Y. Lai, Q.-Y. Cai, and M. S. Zhan, *New J. Phys.* **11**, 113035 (2009).
- ³³K. Burnett, J. B. Watson, A. Sanpera, and P. L. Knight, *Philos. Trans. R. Soc. London A* **356**, 317 (1998).
- ³⁴M. Dörr, *Opt. Express* **6**, 111 (2000).
- ³⁵S. Baier, C. Ruiz, L. Plaja, and A. Becker, *Phys. Rev. A* **74**, 033405 (2006).
- ³⁶Y. Kayanuma, *Phys. Rev. B* **47**, 9940 (1993).
- ³⁷Y. Kayanuma, *Phys. Rev. A* **50**, 843 (1994).
- ³⁸C. Creffield, *Phys. Rev. B* **67**, 165301 (2003).
- ³⁹F. Grossmann, T. Dittrich, P. Jung, and P. Hänggi, *Phys. Rev. Lett.* **67**, 516 (1991).
- ⁴⁰F. Großmann and P. Hänggi, *Europhys. Lett.* **18**, 571 (1992).
- ⁴¹M. Yu. Ivanov and P. B. Corkum, *Phys. Rev. A* **48**, 580 (1993).
- ⁴²M. Yu. Ivanov, P. B. Corkum, and P. Dietrich, *Laser Phys.* **3**, 375 (1993).
- ⁴³V. A. Burdov, *JETP* **85**, 657 (1997).
- ⁴⁴A. Santana, J. M. Gomez Llorente, and V. Delgado, *J. Phys. B* **34**, 2371 (2001).